Available online at www.sciencedirect.com
ScienceDirect
Trans. Nonferrous Met. Soc. China 32(2022) 3623−3634
Transactions of Nonferrous Metals Society of China
www.tnmsc.cn

Microstructure and mechanical properties of Cu/Al joints brazed using (Cu, Ni, Zr, Er)-modified Al−Si filler alloys

Hua-xin LI[1,2,3,4], Ying-dian FENG[1,3,5], Wei-jian SHEN[1,3], Chuan-yang LÜ[1,2,3], Wen-jian ZHENG[1,2,3], Ying-he MA[1,2,3], Gang MA[5], Zhong-ping JIN[5], Yan-ming HE[1,2,3], Jian-guo YANG[1,2,3]

1. Institute of Process Equipment and Control Engineering, Zhejiang □niversity of Technology, Hangzhou 310023, China;
2. Engineering Research Center of Process Equipment and Remanufacturing, Ministry of Education, Zhejiang □niversity of Technology, Hangzhou 310023, China;
3. College of Mechanical Engineering, Zhejiang □niversity of Technology, Hangzhou 310023, China;
4. Innovation Research Institute of Zhejiang □niversity of Technology (Shengzhou), Shengzhou 312400, China;
5. Taizhou Special Equipment Inspection and Testing Research Institute, Taizhou 318000, China

Received 31 August 2021; accepted 14 January 2022

Abstract: To design a promising Al−Si filler alloy with a relatively low melting-point, good strength and plasticity for the Cu/Al joint, the Cu, Ni, Zr and Er elements were innovatively added to modify the traditional Al−Si eutectic filler. The microstructure and mechanical properties of filler alloys and Cu/Al joints were investigated. The result indicated that the Al−Si−Ni−Cu filler alloys mainly consisted of Al(s,s), Al_2(Cu,Ni) and Si(s,s). The Al−10Si−2Ni−6Cu filler alloy exhibited relatively low solidus (521 °C) and liquidus (577 °C) temperature, good tensile strength (305.8 MPa) and fracture elongation (8.5%). The corresponding Cu/Al joint brazed using Al−10Si−2Ni−6Cu filler was mainly composed of $Al_8(Mn,Fe)_2Si$, $Al_2(Cu,Ni)_3$, Al(Cu,Ni), Al_2(Cu,Ni) and Al(s,s), yielding a shear strength of (90.3±10.7) MPa. The joint strength was further improved to (94.6±2.5) MPa when the joint was brazed using the Al−10Si−2Ni−6Cu−0.2Er−0.2Zr filler alloy. Consequently, the (Cu, Ni, Zr, Er)-modified Al−Si filler alloy was suitable for obtaining high-quality Cu/Al brazed joints.

Key words: Cu/Al joint; brazing; Al−Si filler alloy; interface structure; joint strength

1 Introduction

The copper (Cu)/aluminum (Al) hybrid structure is widely used in electronics, heat exchanger and refrigeration industries owing to its low cost, light weight, high specific strength and high electrical conductivity [1−4]. These applications make a reliable joining technology a critical requirement. Recently, the joining technology for Cu/Al dissimilar metals has been developed greatly, including fusion welding [5,6], pressure welding [7,8], brazing [9,10], and so on. Fusion welding requires the welding temperature over the melting-point of base metals, which makes it difficult to obtain a high-quality Cu/Al joint because of the welding defects and intermetallic compounds (IMC) formed during the fusion process. The pressure welding has the ability to produce high-strength Cu/Al hybrid joints, but the pressure required during the joining process makes it inapplicable to flexible Cu/Al components with a complex shape. Compared to the joining methods mentioned previously, brazing technique is adopted

Corresponding author: Yan-ming HE, Tel: +86-15268829978, E-mail: heyanming@zjut.edu.cn;
Jian-guo YANG, Tel: +86-13758194497, E-mail: yangjg@zjut.edu.cn
DOI: 10.1016/S1003-6326(22)66044-8

as the most suitable approach for Cu/Al hybrid structures due to its relatively low joining temperature and pressureless joining process.

The filler alloy is essential to achieving a high-quality brazed joint. The Zn−Al [10,11], Sn−Zn [9], Al−Si [9,12−14] series fillers are commonly used for Cu/Al joints. The Al−Si series fillers are particularly more appliable for Cu/Al hybrid components used in moist outdoor environment compared with Zn−Al and Sn−Zn series fillers due to their high joint strength and excellent corrosion resistance [15,16]. However, the Al−Si series fillers are based on the Al−12.6wt.%Si eutectic alloy with a high eutectic point of 577 °C, usually resulting in the degradation of mechanical properties or even localized melting in some engineering Al alloys during the brazing process. Consequently, extensive research was devoted to designing high-performance Al−Si-based filler alloys satisfying requirements: (1) relatively low melting point, (2) good plasticity for machining, (3) high strength, and (4) excellent corrosion resistance. Generally, metallic Ge, Zn and Cu can be added to effectively reduce the melting-point of Al−Si eutectic alloy. The brittle and expensive Ge makes the Al−Si−Ge filler alloys have a poor processability and inapplicable for commercial applications [12]. The Zn addition tremendously sacrifices the corrosion resistance. The inexpensive Cu appears to be the best option because the Al−Si−Cu filler alloy possesses a relatively low melting point, good processability, high strength and excellent corrosion resistance. Nevertheless, the brittle Al−Cu IMC formed in the filler is a crucial issue that needs to be resolved. For example, CHANG et al [13] studied the brazing of Cu to Al using the Al−Si−Cu fillers with the Cu contents of 10 wt.% and 20 wt.%, and found that a large amount of Al−Cu IMC induced by excessive Cu addition would lead to the degradation of joint strength. To minimize the negative effect of Cu addition, the key is to add some compensating elements to inhibit and/or refine the Al−Cu IMC. It was reported that appropriate Cu replaced by Ni was able to reduce brittleness and improve corrosion resistance of the filler metal, and the Al−Si−Cu−Ni series fillers have been developed for brazing of Al alloy to itself [17,18]. Also, minor Zr, Er, Sc and La commonly act as micro-alloying elements for grain refinement. It was reported that the co-addition of micro-alloying elements in the alloy exhibited superior performances on grain refinement. YANG et al [19] investigated that the effects of minor Er and Zr on microstructure and mechanical properties of Al–Mg–Mn alloy laser welded joints, indicating that the trace elements of Zr and Er could improve the joint tensile strength from 290 to 305 MPa owing to the grain refinement in the fusion zone [19].

In this work, with the purpose of overcoming the drawback of traditional Al−12.6wt.%Si eutectic filler, a novel (Cu, Ni, Zr, Er)-modified Al−Si filler alloy was designed to braze Cu and Al. The Cu element was selected as melting-point depressant, while the Ni element played a role in compensating the negative influence of Cu additive. The Zr and Er were chosen as the micro-alloying elements for grain refinement, especially for brittle IMC. Firstly, the influences of Cu content on the Al−Si−Ni−Cu filler alloys and brazed joints were investigated systematically to obtain optimized Cu content. Subsequently, minor Zr and Er were intentionally added to Al−Si−Ni−Cu filler alloy to improve the joint properties. The microstructure and mechanical properties of Cu/Al brazed joints were studied in detail by the means of scanning electron microscopy (SEM) with energy dispersive X-ray spectroscopy (EDS), hardness and shear test.

2 Experimental

The Al (>99.7%), Si (>99.8%), Cu (>99.9%), Ni (>99.9%), Zr (>99.9%), Er (>99.9%), NaCl (>99.5%) and KCl (>99.5%) were used as the raw materials for the fabrication of filler alloys. Table 1 summarizes the chemical composition of each filler alloy designed in the present work. The filler metals were fabricated by molten salt method. The salt mixture was composed of NaCl and KCl with a mass ratio of 1:1 acting as the reaction medium to prevent the oxidation of the alloy during the melting process. Firstly, the salt mixture was placed in a resistance furnace to melt sufficiently, and then was poured into the crucible containing the metal mixture. Subsequently, the crucible was heated to fully melt the metal mixture, and then was cooled naturally. After that, the filler metals were ultrasonically cleaned to remove the salt mixture. The filler alloy bulks obtained were machined to a 300 μm-thick foil for brazing.

The chemical compositions of as-received Al and Cu base metals were provided in Tables 2 and 3. The as-received Al and Cu bulks were machined to rectangular specimens with the dimensions of 10 mm × 10 mm × 4 mm and 20 mm × 20 mm × 4 mm, respectively. The filler alloy foil, Al and Cu base metals were polished up to 1 μm diamond suspension. Whereafter, the filler alloy foils and Al base metal were chemically etched for 2 min using 5% NaOH chemical solution, and then cleaned in 5% HNO_3 solution for 10 s to clean the oxide on the surface. All specimens were ultrasonically cleaned in an acetone bath for 10 min and then dried in air. The Cu/Al joint was assembled according to the schematic diagram in Fig. 1, where the filler alloy was wrapped with the Noclock brazing flux to avoid the oxidization. The brazing process was carried out in a furnace in air at 590 °C for 10 min. The heating rate was set to be 10 °C/min, and the specimen was cooled in the furnace after brazing.

Table 1 Chemical compositions of Al−10Si−2Ni−*x*Cu (*x*=2, 4, 6, 8, 10) filler alloy (wt.%)

Sample No.	Al	Si	Ni	Cu	Er	Zr
1	86.0	10.0	2.0	2.0	−	−
2	84.0	10.0	2.0	4.0	−	−
3	82.0	10.0	2.0	6.0	−	−
4	80.0	10.0	2.0	8.0	−	−
5	78.0	10.0	2.0	10.0	−	−
6	81.6	10.0	2.0	6.0	0.2	0.2

Table 2 Chemical composition of 3003 aluminum base metal (wt.%)

Al	Si	Fe	Cu	Mn	Zn
≥97	0.6	0.7	0.05−0.20	1.0−1.5	0.1

Table 3 Chemical composition of TP2-Y2 copper base metal (wt.%)

Cu+Ag	Ni	P	Bi	Pb
≥99.85	≤0.01	0.013−0.050	≤0.002	≤0.005

Fe	S	As	Sb	Sn	O
≤0.05	≤0.005	≤0.005	≤0.002	≤0.01	≤0.01

Each of the filler alloys and brazed joints was cut at the middle, and then was polished for microstructural characterization. The microstructure was examined using a field-emission scanning electron microscopy (FE-SEM, S□8010, Hitachi, Japan) equipped with an energy dispersive X-ray spectroscopy (EDS). The solidus and liquidus temperatures of brazing alloys were determined using a thermal analyzer (HCT−1, Beijing Henven Experimental Equipment Co., Ltd., China) for differential scanning calorimetric (DSC) with a heating rate of 10 °C/min in a N_2 atmosphere. The tensile test of filler alloy was carried out according to GB/T 16865—2013 using a universal testing machine (CMT4204, MTS, □SA). The Vickers hardness of the polished specimens was measured by a Vickers indenter (MHVS−1000Z, Shanghai Lidun Instrument Testing Technology Co., Ltd., China). For each indentation, the peak load was set to be 50 g with a dwelling time of 15 s. The brazed specimen was assembled in a custom-built die for shear test using a universal testing machine with a cross-head speed of 0.5 mm/min, and the schematic plot can be found elsewhere [20]. To increase the reliability of the data, at least three samples were tested for tensile and shear strength.

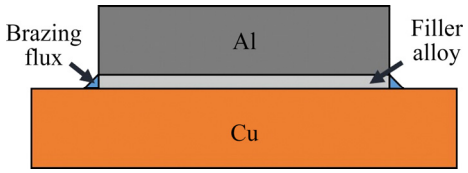

Fig. 1 Schematic diagram of brazing sample assembly

3 Results

3.1 Filler alloy

Figure 2 shows the DSC curves of Al−Si−Ni−Cu filler alloys and corresponding solidus/liquidus temperatures. There was only one obvious endothermic peak for each filler alloy. The start temperature of the endothermic peak represents the solidus temperature (T_i). For the sake of simplicity, the liquidus temperature (T_f) is represented by the temperature of exothermic peak (T_p) [21]. With the increase of Cu content from 2 to 10 wt.%, the liquidus temperature gradually dropped from 583 to 565 °C, while the solidus temperature declined rapidly from 548 to 521 °C, and then remained stable when the Cu content was over 6 wt.%. This fact reveals that the moderate Cu content enabled effective reduction of both liquidus and solidus temperatures, but the excessive Cu content (>6 wt.%) had no significant influence on

the solidus temperature. A reasonable reduction of liquidus/solidus temperatures is beneficial to minimizing the property degradation of Al base metal during brazing process.

Figure 3 shows the typical SEM image, elemental distribution and EDS analysis results on the filler alloy. It can be seen clearly that the Al−10Si−2Ni−2Cu filler alloy mainly consisted of black matrix (A), fishbone-like white phase (B) and needle-like gray phase (C) (Fig. 3(a)). The EDS maps (Figs. 3(b−e)) show that the matrix, white phase and gray phase were rich in Al, Al−Cu−Ni and Si, respectively. Based on the EDS points analysis results (Fig. 3(f)), the black matrix, fishbone-like white phase and needle-like gray phase were determined to be Al(s,s), $Al_2(Cu,Ni)$ and Si(s,s), respectively. There are various Al−Cu IMCs (e.g. Al_2Cu_3, Al_2Cu, AlCu, Al_3Cu_4, Al_4Cu_3 and Al_4Cu_9) according to the equilibrium phase diagram of the Cu/Al system [22]. In the case of Al−Si−Ni−Cu filler alloy with the Cu content below 10 wt.%, the formation of Al_2Cu rather than other Al−Cu IMCs can be explained by the low content of Cu additive. Similar phenomenon was also found in prior study [13].

Figure 4 shows the SEM micrographs of Al−Si−Ni−Cu filler alloys with different Cu contents. It can be seen clearly that all filler alloys were made up of Al(s,s), $Al_2(Cu,Ni)$ and Si(s,s), and the area fraction and grain size of $Al_2(Cu,Ni)$ were varied with the Cu content. Table 4 summarizes the grain size and area fraction of $Al_2(Cu,Ni)$ in the Al−Si−Ni−Cu filler alloys. Note that the grain size and area fraction were calculated by the software

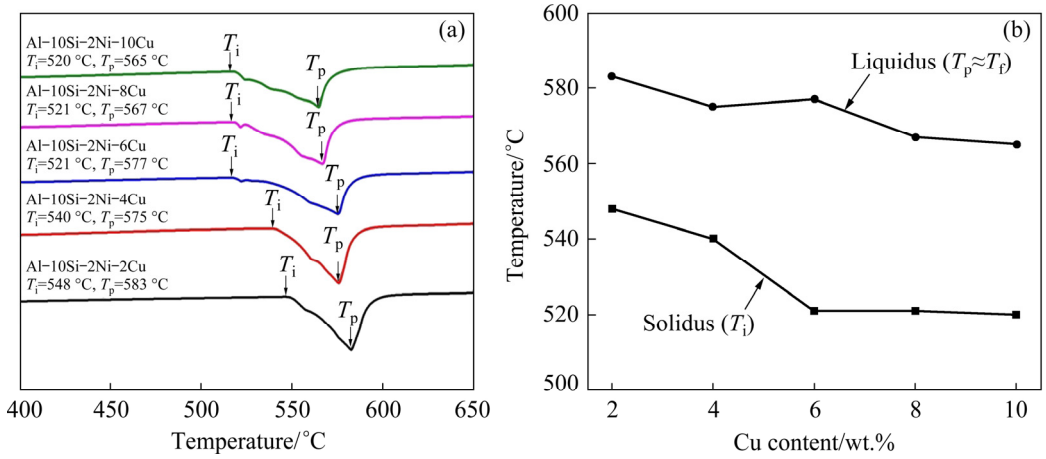

Fig. 2 DSC curves (a) and liquids/solidus temperatures (b) of Al−10Si−2Ni−*x*Cu (*x*=2, 4, 6, 8, 10, wt.%) filler alloys

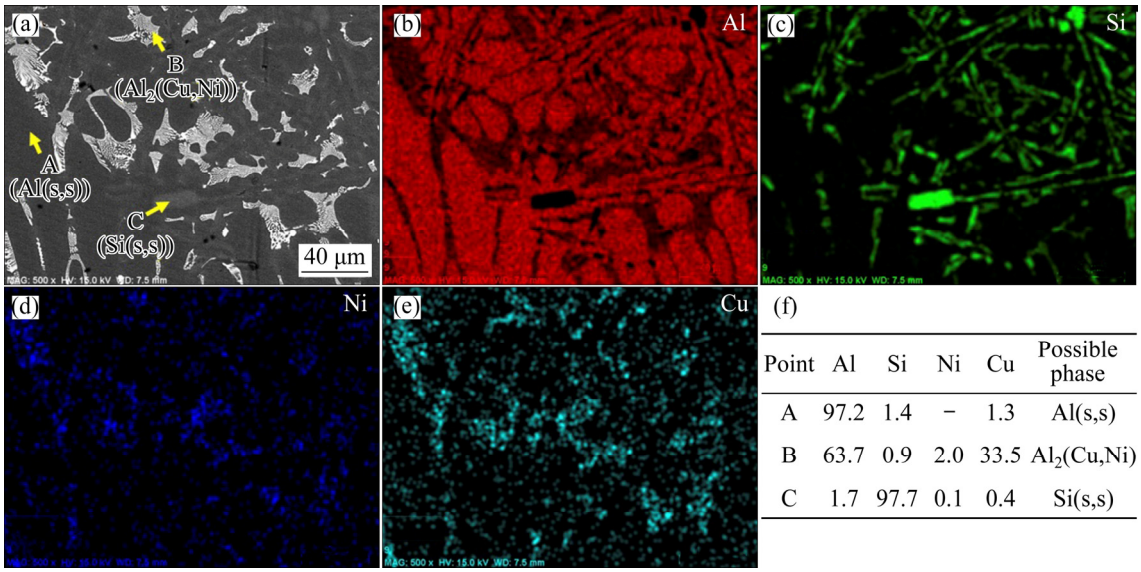

(f)

Point	Al	Si	Ni	Cu	Possible phase
A	97.2	1.4	−	1.3	Al(s,s)
B	63.7	0.9	2.0	33.5	$Al_2(Cu,Ni)$
C	1.7	97.7	0.1	0.4	Si(s,s)

Fig. 3 SEM micrograph (a), elemental distributions (b−e) of Al−10Si−2Ni−2Cu filler alloy and EDS analysis results (f) of points in (a)

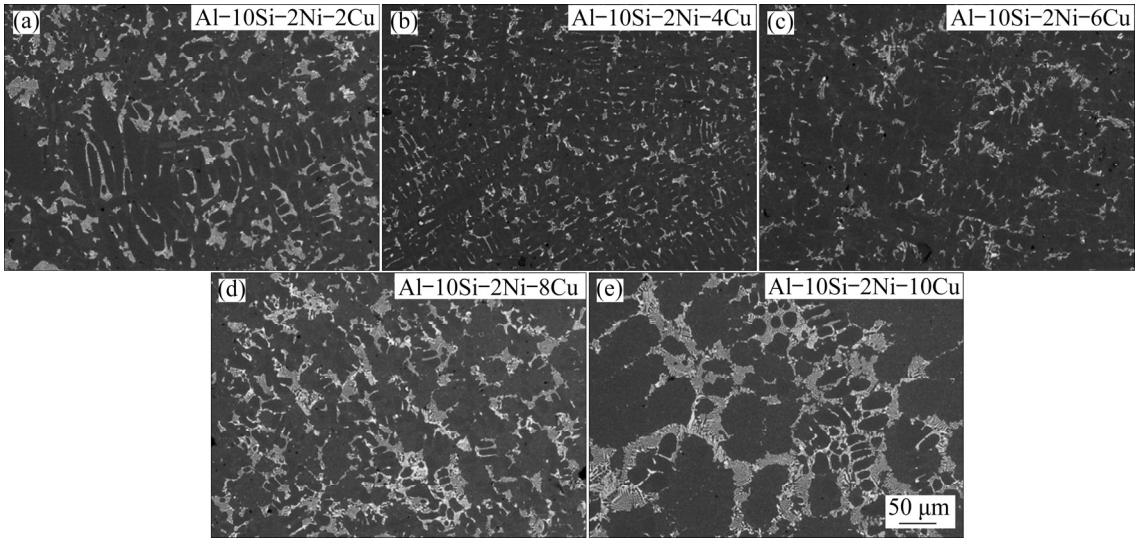

Fig. 4 SEM micrographs of Al−10Si−2Ni−*x*Cu filler alloys: (a) *x*=2; (b) *x*=4; (c) *x*=6; (d) *x*=8; (e) *x*=10

Table 4 Grain size and area fraction of $Al_2(Cu,Ni)$ in Al−10Si−2Ni−*x*Cu filler alloys calculated from Fig. 4

Filler alloy	Minimum grain size/μm	Maximum grain size/μm	Average grain size/μm	Area fraction/%
Al−10Si−2Ni−2Cu	1.15	30.57	4.99	12.6
Al−10Si−2Ni−4Cu	1.04	17.78	2.84	7.1
Al−10Si−2Ni−6Cu	1.07	22.50	3.13	5.8
Al−10Si−2Ni−8Cu	1.67	75.84	5.49	12.88
Al−10Si−2Ni−10Cu	2.51	79.11	7.69	21.87

of Image-pro plus 6.0, and the grain size was defined as the equivalent circle diameter of the fishbone-like $Al_2(Cu,Ni)$. With the increase of Cu content, the average grain size of $Al_2(Cu,Ni)$ decreased from ~5 to ~3 μm, and then increased to ~8 μm. Meanwhile, the area fraction of $Al_2(Cu,Ni)$ decreased from ~12% to ~6%, and then increased to ~22%. The minimum average size and area fraction of brittle $Al_2(Cu,Ni)$ were achieved in the Al−10Si−2Ni−4Cu and Al−10Si−2Ni−6Cu filler alloys, respectively.

Figure 5 shows the tensile strength and fracture elongation of Al−Si−Ni−Cu filler alloys. With the increase of Cu content, the tensile strength increased from 273.6 to 305.8 MPa firstly, and then decreased to 281.3 MPa. The fracture elongation was increased from 7.6% to 9.4%, and then dropped to 5.9%. Al−10Si−2Ni−6Cu filler alloy exhibited the maximum tensile strength (305.8 MPa) and second largest fracture elongation (8.5%), while the Al−10Si−2Ni−4Cu filler alloy possessed the second largest tensile strength (304.6 MPa) and maximum fracture elongation (9.4%). The result implies that

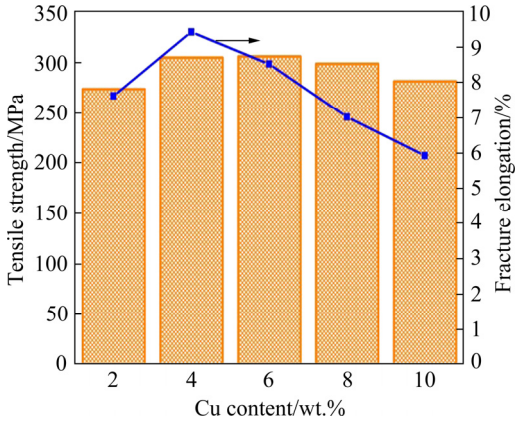

Fig. 5 Tensile strength and fracture elongation of Al−10Si−2Ni−*x*Cu (*x*=2, 4, 6, 8, 10, wt.%) filler alloys

the filler alloy with minimum size and area fraction of brittle $Al_2(Cu,Ni)$ yielded the most excellent strength and plasticity. This is because the crack can easily form and propagate in the brittle $Al_2(Cu,Ni)$ under external pressure applied, thereby resulting in the degradation of strength and plasticity. Therefore, the size and area fraction reductions of brittle $Al_2(Cu,Ni)$ in the filler alloy were in favor of the improvement of strength and plasticity.

3.2 Brazed joint

Figure 6 shows the typical microstructure of Cu/Al joint brazed using Al−10Si−2Ni−6Cu filler alloy. The chemical compositions and possible phases of marked regions in Fig. 6 are summarized in Table 5. In the low-magnification SEM image (Fig. 6(a)), the well-bonded Cu/Al joint was free of crack and disconnection. At the Al/brazing alloy interface (Fig. 6(b)), the gray-black brazing alloy was tightly joined with the black Al base metal without obvious welding defects and transition layers. According to EDS analysis in Table 5, the Al base metal contained Al(s,s) (Phase A) and $Al_6(Mn,Fe)$ (Phase D), while the brazing alloy was composed of Al(s,s) (Phase E), $Al_2(Cu,Ni)$ (Phase B) and $Al_8(Mn,Fe)_2Si$ (Phase C). It should be pointed out that the Mn and Fe elements come from the Al base metal (Table 2), and there is a considerable solid solubility between Mn and Fe [23]. The existence of $Al_8(Mn,Fe)_2Si$ in the brazing alloy instead of Si(s,s) implies that the Mn and Fe elements in the base metal transported to the brazing alloy during brazing process. In the center of brazed seam (Fig. 6(c)), the morphology and phase constitute were similar to those of the edge of brazed seam close to the Al base metal, evidenced by the analogical microstructure in Fig. 6(d) and EDS analysis in Table 5. It should be noted that the grain size of Al−Cu IMC in the seam center was in the range of 0.15−22.07 μm. At the Cu/brazing alloy interface (Fig. 6(d)), the laminar and long strip reaction products were observed at the interface. The EDS analysis shows that Phases K, J, L, I and H were determined to be $Al_2(Cu,Ni)_3$, Al(Cu,Ni), $Al_3(Cu,Ni)_2$, $Al_2(Cu,Ni)$ and Al(s,s), respectively. Among these brittle Al−Cu IMCs, the $Al_2(Cu,Ni)$ had the maximum grain size and area fraction. Therefore, the phase sequence of Cu/brazing alloy interface can be expressed as $Cu/Al_2(Cu,Ni)_3/Al(Cu,Ni)/Al_2(Cu,Ni)/Al(s,s)$. The formation of Al−Cu IMC layer was attributed to the concentration gradient of Cu element at the interface. By taking account of a mass of brittle Al−Cu IMC formed at the Cu/brazing alloy interface, the joint strength of Cu/Al joint was believed to be determined by the Cu/brazing alloy interface, especially brittle $Al_2(Cu,Ni)$.

Figure 7 shows the microstructural evolution of Cu/Al joints brazed using the Al−Si−Ni−Cu filler alloy with different Cu contents. There was no obvious microstructural change at the Al/brazing alloy interface with the increase of Cu content. At the Cu/brazing alloy interface, the thickness of Al−Cu IMC layer was decreased from ~110 to

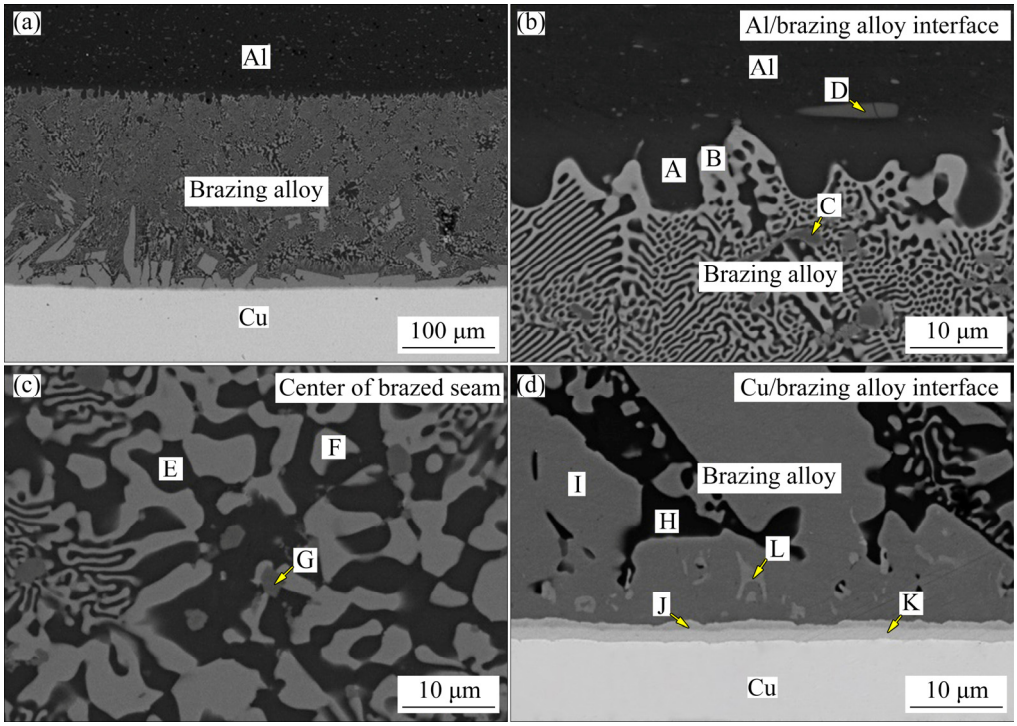

Fig. 6 Cross-sectional SEM micrographs of Cu/Al joints brazed with Al−10Si−2Ni−6Cu filler alloy: (a) Overall appearance; (b) Al/brazing alloy interface; (c) Center of brazed seam; (d) Cu/brazing alloy interface

Table 5 Chemical composition (at.%) and possible phases of marked regions in Fig. 6

Region	Al	Si	Cu	Ni	Mn	Fe	Possible phase
A	94.5	0.5	4.49	−	0.3	0.2	Al(s,s)
B	64.0	0.7	34.4	0.7	−	0.2	$Al_2(Cu,Ni)$
C	68.6	7.5	3.9	0.6	13.5	5.9	$Al_8(Mn,Fe)_2Si$
D	81.8	−	0.8	0.2	9.3	7.9	$Al_6(Mn,Fe)$
E	93.7	0.3	5.8	0.2	−	−	Al(s,s)
F	64.0	0.7	34.5	0.7	−	0.2	$Al_2(Cu,Ni)$
G	71.1	7.7	1.7	0.7	10.2	9.4	$Al_8(Mn,Fe)_2Si$
H	93.9	0.7	5.3	1.4	−	0.1	Al(s,s)
I	65.0	0.6	33.6	0.8	−	−	$Al_2(Cu,Ni)$
J	49.2	−	49.9	1.0	−	−	Al(Cu,Ni)
K	40.7	−	58.6	0.8	−	−	$Al_2(Cu,Ni)_3$
L	59.3	0.1	7.1	33.6	−	−	$Al_3(Cu,Ni)_2$

~33 μm with the increase of Cu content from 2 to 4 wt.%. When the Cu content exceeded 6 wt.%, the Al−Cu IMC layer exhibited a slight reduction in the thickness from ~20 to ~17 μm. In addition, some cracks were observed in the Al−10Si−2Ni−2Cu and Al−10Si−2Ni−4Cu joints. The existence of cracks can be explained by the reasons as follows: (1) The brazing alloy may not fully melt during the brazing process due to the relatively high liquidus/solidus temperature; (2) The thick Al−Cu IMC layer can easily produce the crack owing to the stress concentration.

To refine the brittle Al−Cu IMCs, minor micro-alloying elements of Er and Zr were added into the Al−10Si−2Ni−6Cu filler alloy for brazing, and the joint microstructure is shown in Fig. 8. In the low-magnification SEM image (Fig. 8(a)), the shape of coarse Al−Cu IMC in the Al−10Si−2Ni−6Cu joint (Fig. 6(a)) was evolved from long strip to short rod, accompanied by significant grain refinement. In the high-magnification SEM images (Figs. 8(b−d)), the grain refinement effect induced by micro-alloying was also found in the fishbone-like Al−Cu IMC in the center of the brazing alloy (Fig. 8(c)) and the Al−Cu IMC layer at the Cu/brazing alloy interface (Fig. 8(d)). This is evidenced by the fishbone-like Al−Cu IMC in the seam center with a reduction of the grain size from 0.15−22.07 to 0.15−10.88 μm and the thickness of the Al−Cu IMC layer from ~20 to 10 μm, by comparison of the microstructure before and after the addition of micro-alloying elements. The result reveals that the addition of minor Er and Zr elements enabled effective grain refinement in the brazed seam, which is expected to improve the joint performance. Table 6 summarizes the chemical compositions and possible phases of marked regions in Fig. 8. The possible phases were similar to those obtained in Table 5. The EDS result shows that minor addition of Er and Zr elements would not lead to obvious phase transformation in the brazed seam.

Figure 9 shows the distribution of Vickers hardness across the brazed seam. The hardness of Cu and Al base metals were ~75 and ~40 HV, respectively. With the increase of Cu content in the filler alloys, the hardness of the region from the seam center to the Al side was basically unchanged. On the contrary, the hardness of the brazed seam near the Cu side gradually decreased from ~320 to ~192 HV, which further declined to ~160 HV in the joint brazed using the Al−10Si−2Ni−6Cu−0.2Er−0.2Zr filler alloy. This phenomenon can be explained by the decrescent Al−Cu IMC layer and grain refinement in the Al−Cu IMC (Figs. 7 and 8).

Figure 10 shows the shear strength of Cu/Al alloy joints brazed using different filler alloys. The shear strength showed a good reproducibility. With the increase of Cu content, the joint strength increased from (81.7±8.9) to (90.3±10.7) MPa firstly, and then declined to (86.1±4.2) MPa. The maximum shear strength of (90.3±10.7) MPa was received in the joint brazed using the filler alloy with 6 wt.% Cu. This is because the well-bonded joint was occupied by refined Al−Cu IMC and a thin Al−Cu IMC layer (Fig. 6). The relatively low joint strength obtained in the joints with 2 and 4 wt.% Cu was due to the cracks formed at the Cu/brazing alloy interface (Figs. 7(a−d)). It is widely accepted that the crack may act as a stress concentration site to cause the early failure of joint under an external pressure applied, thus resulting in the degradation of joint strength. The reduction of joint strength when the Cu content was over 6 wt.% can be explained by the enhanced brittleness in the filler alloys (Fig. 5). The Cu/Al joint brazed with minor Er and Zr added to the Al−10Si−2Ni−6Cu filler alloy exhibited the highest shear strength of (94.6±2.5) MPa, which was increased by 5% approximately in comparison with the joint brazed without Er and Zr. The improved joint strength

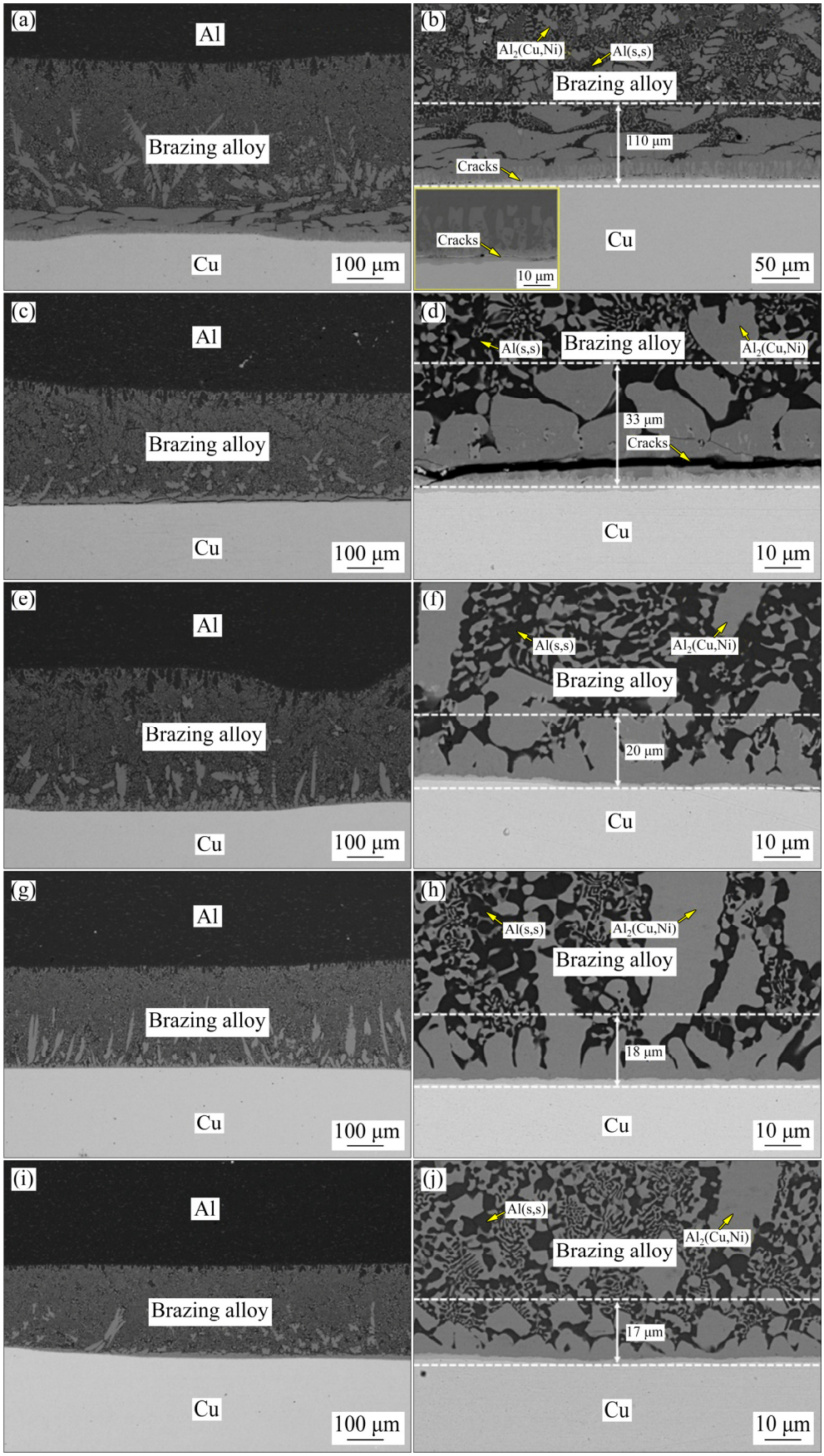

Fig. 7 Cross-sectional SEM micrographs of Cu/Al joints brazed with Al−10Si−2Ni−*x*Cu filler alloys: (a, b) 2 wt.% Cu; (c, d) 4 wt.% Cu; (e, f) 6 wt.% Cu; (g, h) 8 wt.% Cu; (i, j) 10 wt.% Cu

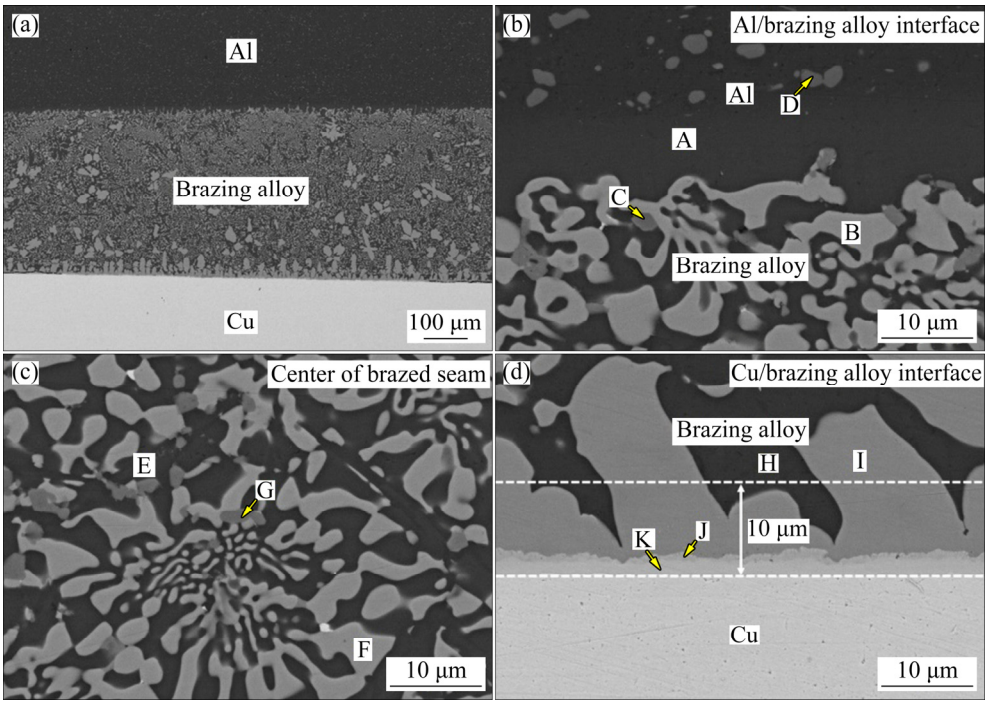

Fig. 8 Cross-sectional SEM micrographs of Cu/Al joints brazed with Al−10Si−2Ni−6Cu−0.2Er−0.2Zr filler alloy: (a) Overall appearance; (b) Al/brazing alloy interface; (c) Center of brazed seam; (d) Cu/brazing alloy interface

Table 6 Chemical composition (at.%) and possible phases of marked regions in Fig. 8

Region	Al	Si	Cu	Ni	Mn	Fe	Possible phase
A	95.8	0.1	3.6	0.3	0.2	–	Al(s,s)
B	66.9	0.7	31.5	0.8	0.1	–	$Al_2(Cu,Ni)$
C	74.7	5.1	0.8	0.2	10.3	8.9	$Al_8(Mn,Fe)_2Si$
D	85.4	–	0.1	–	8.1	6.4	$Al_6(Mn,Fe)$
E	94.8	0.2	4.8	0.2	–	–	Al(s,s)
F	65.8	0.7	32.6	0.8	0.1	0.1	$Al_2(Cu,Ni)$
G	72.7	6.9	5.5	0.7	8.7	7.4	$Al_8(Mn,Fe)_2Si$
H	92.8	0.4	5.3	1.4	–	0.1	Al(s,s)
I	64.6	0.7	34.5	0.8	–	–	$Al_2(Cu,Ni)$
J	50.6	–	48.7	0.8	–	–	Al(Cu,Ni)
K	39.9	–	59.6	0.5	–	–	$Al_2(Cu,Ni)_3$

was attributed to the grain refinement and thinner Al−Cu IMC layer induced by micro-alloying elements (Figs. 6 and 8).

Figure 11 shows typical fracture morphology and mode of Cu/Al alloy joints. It can be seen clearly that the fracture surface was accompanied by river patterns, as a representative of brittle fracture (Figs. 11(a−c)). The fracture mode implied that the fracture happened at the region close to the Cu/brazing alloy interface (Fig. 11(d)), suggesting

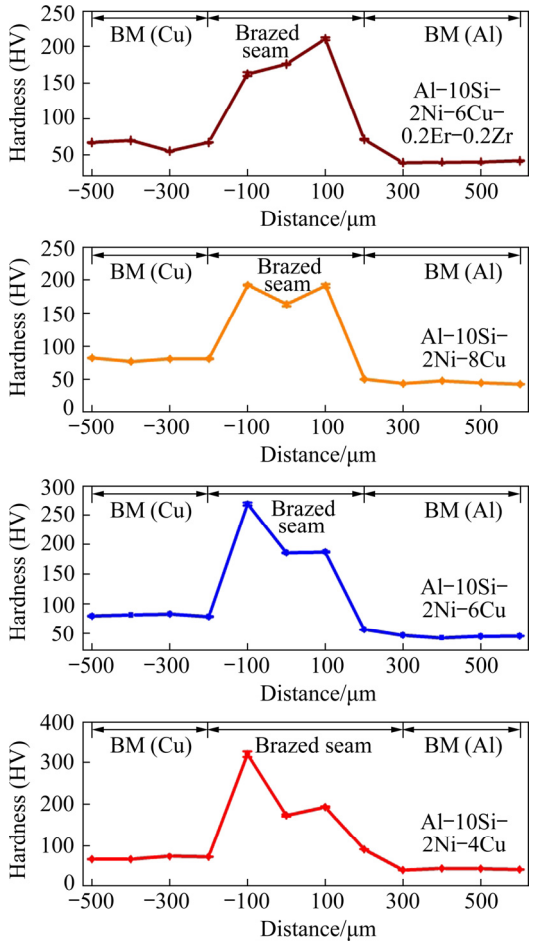

Fig. 9 Distribution of Vickers hardness across brazed seam

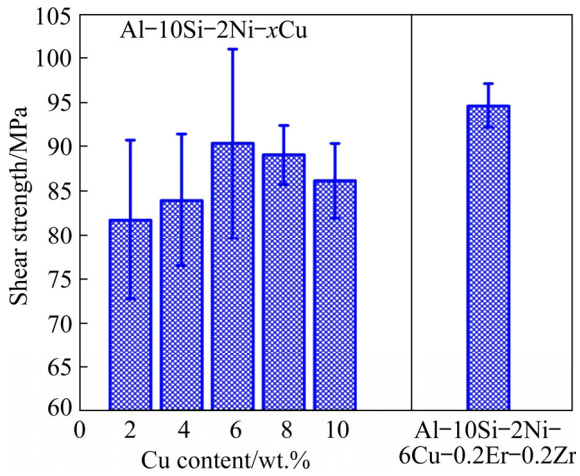

Fig. 10 Shear strength of Cu/Al joints brazed with Al−10Si−2Ni−*x*Cu (*x*=2, 4, 6, 8, 10, wt.%) and Al−10Si−2Ni−6Cu−0.2Er−0.2Zr filler alloys

that this region was the weakest part in the joint. This is because the brittle Al−Cu IMC and crack were easily formed in this region.

4 Discussion

A desirable (Cu, Ni, Zr, Er)-modified Al−Si filler alloy requires to enable a relatively low melting-point and fine/less brittle Al−Cu IMC. The effects of these elements on the filler alloy and brazed joint are illustrated as follows. The Cu plays a key role in the composite filler, because Cu element can not only reduce the melting-point, but also produce brittle Al−Cu IMC. Appropriate Cu enable effective reduction of solidus and liquidus temperatures, but excessive Cu is unable to lower the solidus temperature (Fig. 2). This is caused by the formation Al−32.7wt.%Cu eutectic alloy with a relatively low melting point of 548 °C [22], similar to the previous work [13]. The Cu content has significant effect on the microstructure of filler alloys and brazed joints. In the filler alloys, the area fraction and grain size of Al−Cu IMC decreased first and then increased with the increase of Cu content (Fig. 4). This is because appropriate Cu can significantly enhance the nucleation sites of Al−Cu IMC, thereby resulting in the grain refinement. When the Cu content is superfluous, the nucleation sites will not increase remarkably, but the excess Cu is inevitable to enlarge the area fraction and size of Al−Cu IMC. In the brazed joints, the thickness of the Al−Cu IMC layer at the Cu/brazing alloy interface gradually decreased with the increase of Cu content in the filler alloy (Fig. 7). It should be pointed out that the formation of the Al−Cu IMC layer is attributed to the Cu element from the Cu base metal. Thus, enhanced Cu content in the filler alloy may limit the transportation of Cu element

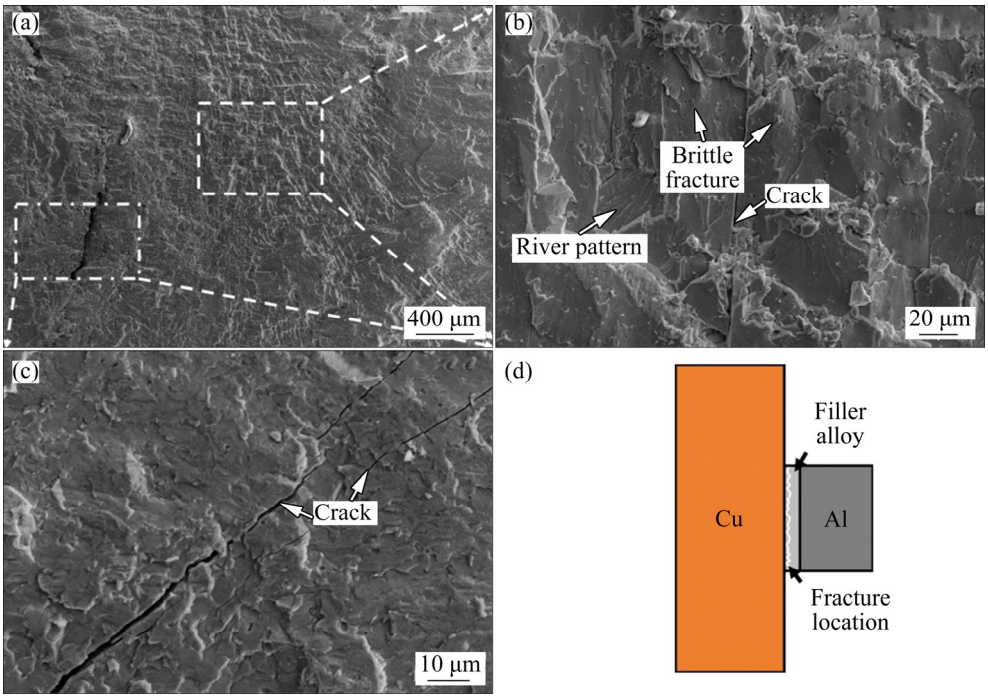

Fig. 11 Typical fracture morphology and mode of Cu/Al alloy joints brazed with Al−10Si−2Ni−2Cu filler alloy at 590 °C for 10 min: (a−c) Typical fracture morphology; (d) Schematic plot of fracture mode

from the Cu base metal to the brazing alloy. In our original motivation, the Ni element is expected to act as compensating element to reduce the negative effect of Cu. Based on the EDS result (Tables 5 and 6), the Ni element was concentrated in the Al−Cu IMC. By taking account of the solid solution between Ni and Cu according to the Cu−Ni binary phase diagram [24], the replacement of minor Cu in brittle Al_2Cu by Ni via solid solution is expected to reduce the brittleness of filler alloy. The significant grain refinement was observed in the brazed joint with the addition of minor Er and Zr (Fig. 8). The result indicates that minor Er and Zr act as effective micro-alloying elements for grain refinement as expected. Consequently, the Al−Si filler alloy modified by Cu, Ni, Zr and Er is able to effectively reduce its low melting-point, and simultaneously restrain the negative effect of brittle Al−Cu IMC.

5 Conclusions

(1) The Al−Si−Ni−Cu series filler alloys mainly consisted of Al(s,s), Al_2(Cu,Ni) and Si(s,s). The optimal Cu content was determined to be 6 wt.%, in which the Al−10Si−2Ni−6Cu filler alloy exhibited the lowest solidus temperature of 521 °C, relatively refined Al_2(Cu,Ni), maximum tensile strength of 305.8 MPa and second largest fracture elongation of 8.5%.

(2) The phase constitute of brazed seam was mainly composed of $Al_8(Mn,Fe)_2Si$, $Al_2(Cu,Ni)_3$, Al(Cu,Ni), Al_2(Cu,Ni) and Al(s,s). The maximum joint strength of (94.6±2.5) MPa was obtained in the Cu/Al joint brazed at 570 °C for 10 min using the Al−10Si−2Ni−6Cu−0.2Er−0.2Zr filler. The excellent joint strength was attributed to the crack-free interface, less brittle Al−Cu IMC and grain refinement effect in the brazed joint.

Acknowledgments

The authors appreciate the financial support from the Primary Research & Development Plan of Zhejiang Province, China (No. 2021C01178), the National MCF Energy R&D Program, China (No. 2019YFE03100400), the National Natural Science Foundation of China (Nos. 51705457, 51975530, 52005445, 52175368), and the Natural Science Foundation of Zhejiang Province, China (Nos. LQ21E050015, LQ21E050018).

References

[1] JI Feng, X□E Song-bai, LO□ Ji-yuan, LO□ Yin-bin, WANG Shui-qing. Microstructure and properties of Cu/Al joints brazed with Zn−Al filler metals [J]. Transactions of Nonferrous Metals Society of China, 2012, 22(2): 281−287.

[2] LEE S, LEE M G, LEE S P, LEE G A, KIM Y B, LEE J S, BAE D S. Effect of bonding interface on delamination behavior of drawn Cu/Al bar clad material [J]. Transactions of Nonferrous Metals Society of China, 2012, 22(3): s645−s649.

[3] QIAN Xiang-fei, G□O Qiao-neng, YANG Shi-e, WANG Ming-xing, LI□ Qiang, WANG Jie-fang. Molecular dynamics simulation of interface bonding and tensile properties of Cu/Al casting [J]. The Chinese Journal of Nonferrous Metals, 2020, 30(12): 2886−2900.

[4] DING Hai-min, MIAO Wen-zhi, H□ANG Xiao-wei, LI□ Qing, FAN Xiao-liang, WANG Hui-qiang, CH□ Kai-yu, LI Chun-yan. Influence of Al addition on microstructures of Cu−B alloys and Cu−ZrB_2 composites [J]. Transactions of Nonferrous Metals Society of China, 2020, 30(5): 1335−1346.

[5] MAI T A, SPOWAGE A C. Characterisation of dissimilar joints in laser welding of steel–kovar, copper–steel and copper–aluminium [J]. Materials Science and Engineering A, 2004, 374: 224−233.

[6] SOLCHENBACH T, PLAPPER P. Mechanical characteristics of laser braze-welded aluminium–copper connections [J]. Optics and Laser Technology, 2013, 54: 249−256.

[7] AVETTAND-FENOEL M N, RACINE□X G, DEBE□GNY L, TAILLARD R. Microstructural characterization and mechanical performance of an AA2024 aluminium alloy–pure copper joint obtained by linear friction welding [J]. Materials & Design, 2016, 98: 305−318.

[8] SINHA V C, K□ND□ S, CHATTERJEE S. Microstructure and mechanical properties of similar and dissimilar joints of aluminium alloy and pure copper by friction stir welding [J]. Perspectives in Science, 2016, 8: 543−546.

[9] Y□ Hua, ZHANG Liang-liang, CAI Fang-fang, ZHONG Su-juan, MA Jia, ZHANG Yi, SI An-heng, WEI Shi-zhong, LONG Wei-min, STOCK H R, OSAKA A. Interface microstructure and growth mechanism of brazing Cu/Al joint with BAl88Si filler metal [J]. Vacuum, 2020, 181: 109641.

[10] JI Feng, X□E Song-bai. Growth behaviors of intermetallic compound layers in Cu/Al joints brazed with Zn−22Al and Zn−22Al−0.05Ce filler metals [J]. Materials & Design, 2013, 51: 907−915.

[11] YE Zheng, YANG Hao, H□ANG Ji-hua, YANG Jian, CHEN Shu-hai. A novel Zn−Al−Si corrosion resistant filler metal for Cu/Al brazing [J]. Materials Letters, 2017, 206: 201−204.

[12] NI□ Zhi-wei, YE Zheng, LI□ Kai-kai, H□ANG Ji-hua, CHEN Shu-hai, ZHAO Xing-ke. Microstructure and property of Cu/Al joint brazed with Al−Si−Ge filler metal [J]. Acta Metallurgica Sinica, 2017, 53(6): 719−725.

[13] CHANG S Y, TSAO L C, LI T Y, CH□ANG T H. Joining 6061 aluminum alloy with Al−Si−Cu filler metals [J].

Journal of Alloys and Compounds, 2009, 488: 174−180.
[14] CH□ANG T H, TSAO L C, TSAI T C, YEH M S , W□ C S. Development of a low-melting-point filler metal for brazing aluminum alloys [J]. Metallurgical and Materials Transactions A, 2000, 31(9): 2239−2245.
[15] MAO Zhi-ping, XIE Jing-pei, WANG Ai-qin, WANG Wen-yan, LI Yan, MA Dou-qin. Interfacial microstructure and bonding strength of copper/aluminum clad sheets produced by horizontal twin-roll casting and annealing [J]. Materials Research Express, 2018, 6(1): 016505.
[16] YANG Min-xuan, HE Peng, LIN Tie-song. Effect of brazing conditions on microstructure and mechanical properties of Al_2O_3/Ti−6Al−4V alloy joints reinforced by TiB whiskers [J]. Journal of Materials Science and Technology, 2013, 29(10): 961−970.
[17] ZHANG Guo-wei, BAO Ye-feng, JIANG Yong-feng, ZH□ Hong. Microstructure and mechanical properties of 6063 aluminum alloy brazed joints with Al−Si−Cu−Ni−RE filler metal [J]. Journal of Materials Engineering and Performance, 2011, 20(8): 1451−1456.
[18] PEI Chong, W□ Xin, ZHANG Guo-qing, CHENG Yao-yong, REN Xin-yu, WANG Wei, XIONG Hua-ping. Microstructures and mechanical properties of brazed 6063 aluminum alloy joint with Al−Cu−Si−Ni filler metal [J]. Welding in the World, 2020, 64(3): 1933−1938.
[19] YANG Dong-xia, LI Xiao-yan, HE Ding-yong, H□ANG Hui. Effect of minor Er and Zr on microstructure and mechanical properties of Al−Mg−Mn alloy (5083) welded joints [J]. Materials Science and Engineering A, 2013, 561: 226−231.
[20] LI Hua-xin, SHEN Wei-jian, CHEN Wei-jian, WANG Wei-zheng, LI□ Guo-hao, L□ Chuan-yang, ZHENG Wen-jian, MA Ying-he, YANG Jian-guo, DING Zhen-yu, ZO□ Hai, HE Yan-ming. Microstructural evolution and mechanical properties of AlCoCrFeNi high-entropy alloy joints brazed using a novel Ni-based filler [J]. Journal of Alloys and Compounds, 2021, 860: 157926.
[21] BANDA W, GEORGALLI G A, LANG C, EKSTEEN J J. Liquidus temperature determination of the Fe−Co−Cu system in the Fe-rich corner by thermal analysis [J]. Journal of Alloys and Compounds, 2008, 461: 178−182.
[22] LI□ X J, OHN□MA I, KAIN□MA R, ISHIDA K. Phase equilibria in the Cu-rich portion of the Cu−Al binary system [J]. Journal of Alloys and Compounds, 1998, 264: 201−208.
[23] WIT□SIEWICZ V T, SOMMER F, MITTEMEIJER E J. Reevaluation of the Fe−Mn phase diagram [J]. Journal of Phase Equilibria and Diffusion, 2004, 25(4): 346−354.
[24] SOPO□SEK J, VRESTAL J, PINKAS J, BROZ P, B□RSIK J, STYSKALIK A, SKODA D, ZOBAC O, LEE J. Cu−Ni nanoalloy phase diagram–Prediction and experiment [J]. Calphad, 2014, 45: 33−39.

(Cu, Ni, Zr, Er)改性的 Al−Si 钎料钎焊 Cu/Al 接头的显微组织和力学性能

李华鑫[1,2,3,4]，冯印典[1,3,5]，沈伟健[1,3]，闾川阳[1,2,3]，
郑文健[1,2,3]，马英鹤[1,2,3]，马 刚[5]，金仲平[5]，贺艳明[1,2,3]，杨建国[1,2,3]

1. 浙江工业大学 化工机械设计研究所，杭州 310023；
2. 浙江工业大学 过程装备及其再制造教育部工程研究中心，杭州 310023；
3. 浙江工业大学 机械工程学院，杭州 310023；
4. 嵊州市浙江工业大学创新研究院，嵊州 312400；
5. 台州市特种设备检验检测研究院，台州 318000

摘 要：为了设计一种具有较低熔点、较好强度和塑性的 Al−Si 钎料钎焊 Cu/Al 接头，创新性地提出添加 Cu、Ni、Zr 和 Er 等元素对传统的 Al−Si 共晶钎料进行改性。对改性的 Al−Si 钎料及其 Cu/Al 钎焊接头的显微组织与力学性能进行研究。结果表明，Al−Si−Ni−Cu 钎料主要由 Al(s,s)、Al_2(Cu,Ni)和 Si(s,s)组成。Al−10Si−2Ni−6Cu 钎料合金具有较低的固相线(521 ℃)和液相线(577 ℃)温度、良好的抗拉强度(305.8 MPa)和断后伸长率(8.5%)。Al−10Si−2Ni−6Cu 钎料钎焊的 Cu/Al 接头主要由 Al_8(Mn,Fe)$_2$Si、Al_2(Cu,Ni)$_3$、Al(Cu,Ni)、Al_2(Cu,Ni)和 Al(s,s)组成，其剪切强度为(90.3±10.7) MPa。当采用 Al−10Si−2Ni−6Cu−0.2Er−0.2Zr 钎焊 Cu/Al 时，接头强度可以进一步提升到(94.6±2.5) MPa。因此，(Cu, Ni, Zr, Er)改性的 Al−Si 钎料可以用于制备高质量的 Cu/Al 钎焊接头。

关键词：Cu/Al 接头；钎焊；Al−Si 钎料；界面结构；接头强度

(Edited by Bing YANG)